Phenanthrenequinone-Based Linear Polymers as Sustainable Cathode Materials for Rechargeable Li-Ion Batteries

Xinya Guo[1], Ying Zhang[1], Han Chen[1], Chaohui Cui[2], Zhenyao Li[1], Ya Du[2,],
Baofeng Wang[1,*] and Haishen Yang[1,*]*

[1] Shanghai Key Laboratory of Materials Protection and Advanced Materials in Electric Power, College of Environmental and Chemical Engineering, Shanghai University of Electric Power, Shanghai 200090, China.
[2] Institute of Advanced Synthesis, School of Chemistry and Molecular Engineering, Nanjing Tech University, Nanjing 211816, China.
[*]E-mail: yanghsh@shiep.edu.cn (H. Yang), wangbaofeng@shiep.edu.cn (B. Wang),
ias_ydu@njtech.edu.cn (Y. Du)

Coal tar is a useful industrial by-product, which is produced in large quantities every year, but has not been adequately utilized thus far. Herein, we design and synthesize two novel coaltar-derived organic linear polymers, namely, poly(2-ethynylphenanthrene-9,10-dione) (PEPQ) and poly(2-(thiophen-2-yl)phenanthrene-9,10-dione) (PTPQ). Beyond as traditional anode materials from coal tar, PEPQ and PTPQ were studied as lithium (Li)-ion battery (LIB) cathode materials in this study. The obtained PEPQ and PTPQ exhibited reversible specific capacities of up to 125 and 138 mAh g^{-1}, respectively, at 10 mA g^{-1}, in LIBs. In particular, the comparative study on the electrochemical performance of these two polymers revealed that replacing the ethynylene linkage (in PEPQ) with thiophene linkage (in PTPQ) endowed the material with faster redox kinetics, a greater electronic conductivity, and thus a higher active site utilization (75% vs. 54%). This discovery in this work could provide elementary insights into the rational construction of organic cathode materials for LIBs with a superior performance.

Keywords: Coal Tar, Linear Conjugated Polymer, Lithium Ion Batteries, Organic Cathode Material.

1. INTRODUCTION

It is highly desirable to develop eco-friendly batteries with low cost and abundant resources to extensively utilization of electricity generated from renewable energies and generalization of green electric vehicles. Rechargeable lithium (Li)-ion batteries (LIBs) based on organic electrode materials
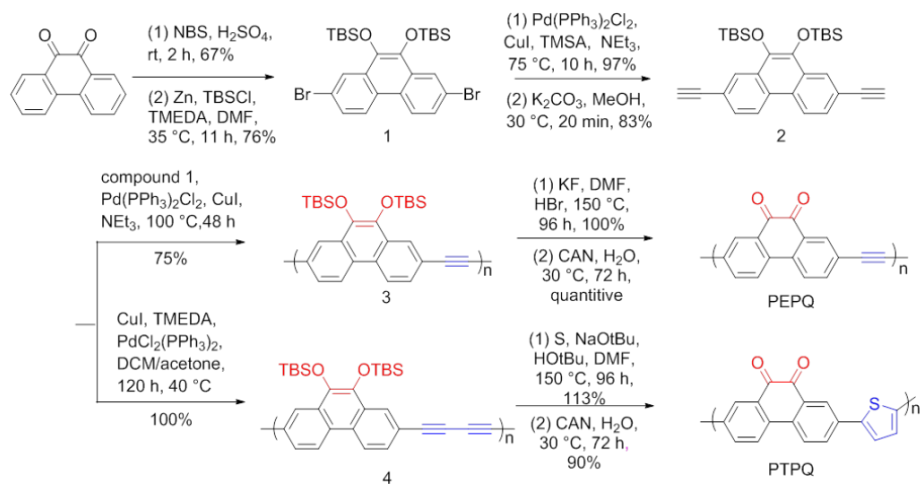
are considered the most promising competitors [1]. In contrast to inorganic cathode materials, organic cathode materials have major advantages, such as eco-friendliness [2], abundant resources [3], facile processability, easy recyclability and disposability [4]. Among organic cathode materials, organic carbonyl compounds (OCCs) are considered to be the most favourable LIB class owing to their outstanding comprehensive performance [5]. Numerous OCCs have been reported, and phenanthrenequinone (PQ) is one of the most important members because of its high potential (2.61 V) and higher energy density [6]. Most importantly, PQ is environmentally sustainable because of its derivation from coal tar, a major by-product with huge production from coal coking and coal gasification processes. The substitution of traditional cathode materials with coal tar or its derivatives could mitigate the environmental pollution caused by the direct burning of coal tar, and promote the construction of a sustainable society [7]. However, most of these chemicals/derivatives encounter the problem of dissolution in organic electrolytes, thus causing a sharp decay in cycle stability [8]. Different approaches have been developed to manage this issue [9-17]. Another challenge is the low intrinsic electrical conductivity, resulting slow redox kinetics and low active-site utilization. This problem can be alleviated by composition with conductive materials [18, 19], or by molecular design [20, 21]. Our approach herein is to design and synthesize insoluble phenanthrenequinone-based polymers with linear ethynylene/thiophene-alternated conjugated architectures. The conjugated structure facilitates efficient electron transportation along the main chain [22]. Furthermore, the incorporation of chalcogen atoms into the structural backbone will be probed with the hope of further enhancing the charge-carrier mobility [23].

In this work, we utilized PQ, a derivative of phenanthrene in coal tar [24], as a starting material to synthesize two novel organic polymeric cathodes, namely, poly(2-ethynylphenanthrene-9,10-dione) (PEPQ) and poly(2-(thiophen-2-yl)phenanthrene-9,10-dione) (PTPQ), for LIBs. PTPQ with thiophene linkage demonstrated superior performance than PEPQ with ethynylene linkage, indicating the advantages of organic electrode materials functionalized alternatively with P/N functional groups.

2. EXPERIMENTAL

2.1 Synthesis

PEPQ and PTPQ were prepared from commercially available PQ, as shown in Scheme 1. Bromination of PQ with NBS/H_2SO_4 produced dibromophenanthrenequinone, followed by the reduction and then protection to generate silyl ether 1. This protection-deprotection strategy is necessary to avoid catalyst deactivation by orthodiketones [14] and to improve the monomer solubility, thus possibly improving the degree of polymerization of PEPQ and PTPQ. Diethynylphenanthrene 2 was yielded by Sonogashira coupling with ethynyltrimethylsilane followed by desilylation in the presence of potassium carbonate. With intermediate 2 in hand, PEPQ was produced by the Sonogashira coupling of 1 and 2, deprotection, and oxidation with ceric ammonium nitrate (CAN). PTPQ was prepared through the homocoupling of 4 and then oxidation-deprotection with CAN. All synthesis details are provided in the Supplementary Information.

Scheme 1. Synthetic routes of cathode materials PEPQ and PTPQ.

2.2 Characterization of PEPQ and PTPQ

Fourier transform infrared (FTIR) spectra were acquired from PerkinElmer Spectrum Two FT-IR in range of 400-4000 cm^{-1}. Thermogravimetric (TG) analysis was tested on the NETZSCH STA 409 PC/PG apparatus within temperature range of 26-800 °C with a heating rate of 10 °C min^{-1} under nitrogen. Elemental analysis was accomplished on the Elementar Vario EL cube. Scanning electron microscopes (SEM) was measured on JEOL JSM-7810F. Liquid ^{1}H NMR and ^{13}C NMR spectrum were acquired on a Bruker AVANCE III 400M. Solid-state ^{13}C cross-polarization/magic angle spinning (CP/MAS) nuclear magnetic resonance (NMR) spectrum was performed on an Agilent 600M.

2.3 Electrochemical tests

To conduct electrochemical measurements, Standard CR-2016 coin-type half cells were assembled in a glove box filled with argon (H$_2$O<0.01 ppm, O$_2$<0.01 ppm). The device consists of a working electrode, Celgard 2400 membrane, nickel foam and stainless steel positive and negative shell. The electrolyte used in the batteries is 1 M LiTFSI-DOL/DME (V$_{DOL}$/V$_{DME}$ = 1:1). For each coin cell, 0.25 mL of electrolyte was added. The working electrode was prepared as follows, the weight ratio of active materials (PEPQ or PTPQ) to conductive carbon material (multi-wall carbon nanotubes, MWCNTs) to binder (polyvinylidene fluoride, PVDF) was set to 3: 5: 2. The mixture was ball milled into a slurry at room temperature for 2 h. The prepared slurry was coated onto carbon-coated aluminium foil and then dried at 80 °C for 24 h in vacuo. The dried electrode materials were cut into discs (14 mm in diameter), and the typical loadings were approximately 1.2 and 0.8 mg cm^{-2}. The cells were placed in the glove box for an equilibration time of 24 h before testing. The galvanostatic charge/discharge tests were performed on a NEWARE CT-4008 cell test instrument (Shenzhen, China) at room temperature. Cyclic voltammetry (CV) tests and electrochemical impedance spectroscopy (EIS) were recorded on the electrochemical workstation system (PGSTAT302N AutoLab, Metrohm, Switzerland).

3. RESULTS AND DISCUSSION

Figure 1 shows the FTIR spectra of six major compounds. Regarding PQ, three representative absorption peaks at 1670 cm^{-1} (C=O stretching vibration), 1280 cm^{-1} (C−O stretching vibration of the aromatic skeleton), and 765 cm^{-1} (C−H out-of-plane deformation vibration of the aromatic skeleton) were observed [3]. For compound 2, absorption peaks at 3280 cm^{-1} (≡C−H stretching vibration), 2100 cm^{-1} (C≡C stretching vibration), 2940 cm^{-1}, 2860 cm^{-1} (C−H stretching vibration of the methyl group), and 831 cm^{-1} (C−H out-of-plane deformation vibration of the aromatic skeleton) were observed. No notable carbonyl absorption peak was observed at 1670 cm^{-1}, indicating that the carbonyl group was successfully protected. In contrast to the spectrum of the precursor 2, the typical absorption peaks of H−C(C≡C) disappeared in the FTIR spectrum of compound 3, indicating the complete replacement of the terminal alkyne hydrogen by compound 1. In the FT-IR spectrum of PEPQ, the disappearance of the characteristic C−H vibration bands of the methyl group and the reappearance of the characteristic C=O vibration bands indicated that its active sites had been successfully released. For PTPQ, stretching vibration peaks of C−S−C in its thiophene rings at approximately 1050 cm^{-1} and C=O at approximately 1673 cm^{-1} were found. To further confirm the structure of PTPQ and the degree of reaction of compound 4, compound 4 and PTPQ were characterized by solid-state ^{13}C CP/MAS NMR spectra (Figure S1). The signals from 115 to 145 ppm in PTPQ correspond to the carbon atoms in the thiophene rings, which is consistent with a related report [25], and through the comparison of the two spectra, we concluded that compound 4 was mostly converted into PTPQ. Next, the thermal stabilities of PEPQ and PTPQ were analysed by TGA under a nitrogen atmosphere. As shown in Figure S2, at a 10% weight loss, the polymers remained thermally stable up to 442 and 192 °C respectively, indicating that both PEPQ and PTPQ, respectively, attained a good thermal stability. The surface morphology of PEPQ and PTPQ was characterized by scanning electron microscopy. As shown in Figure S3, the morphology of the two materials resembled irregular stacks. The element mapping images of PTPQ showed that the C, O, and S elements were evenly distributed in the material.
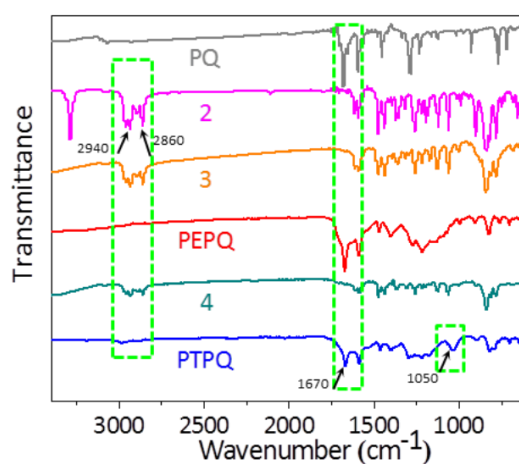

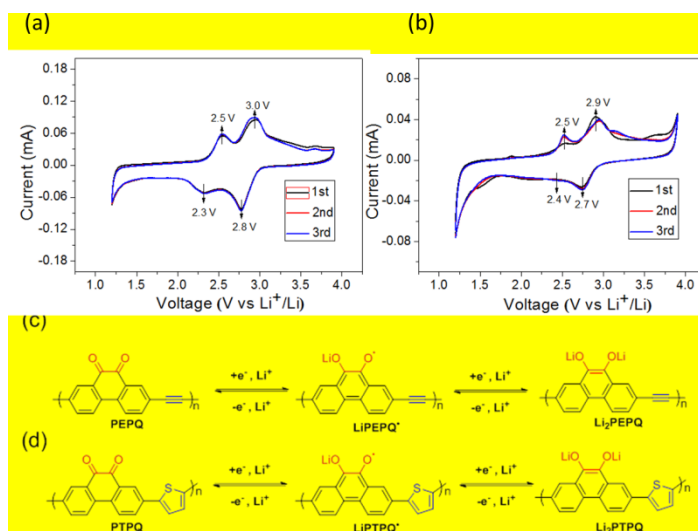
Figure 1. FTIR spectra of six major compounds.

Figure 2. (a) and (b) CV measurements of PEPQ and PTPQ, respectively, at 0.5 mV s^{-1}. (c) and (d) Theoretical working mechanisms for cathode materials PEPQ and PTPQ, respectively.

To study the electrochemical reaction mechanisms, the cyclic voltammetry (CV) test results of these two cathode materials are shown in Figure 2a-b. Attributed to their redox-active PQ moieties, PEPQ and PTPQ are supposed to form radical anions and dianions through the stepwise reduction of carbonyl groups by a two-electron transfer process to form Li$_2$PEPQ and Li$_2$PTPQ, respectively (discharge process). The resultant lithium enolates gradually release two lithium ions, which return to their original states through oxidation (charge process) (Figure 2c-d). PEPQ and PTPQ exhibit two pairs of redox peaks between 4.0 and 1.2 V and between 3.9 and 1.2 V, respectively. The first pair of reduction/oxidation peaks (2.8/3.0 V for PEPQ, and 2.7/2.9 V for PTPQ) correlates to the insertion/de-insertion of the first lithium ion, which is accompanied by the structural transition between one carbonyl group and lithium enolate. The second pair of reduction/oxidation peaks (2.3/2.5 V for PEPQ, and 2.4/2.5 V for PTPQ) correlates to the insertion/de-insertion of the second lithium ion, which is accompanied by the structural transition between another carbonyl group and lithium enolate [26]. More importantly, compared to PEPQ, PTPQ shows a narrower peak separation of the anodic and cathodic peaks, which is attributed to its high electrode reaction rate and power capability in the discharge-charge process of the LIB [27].
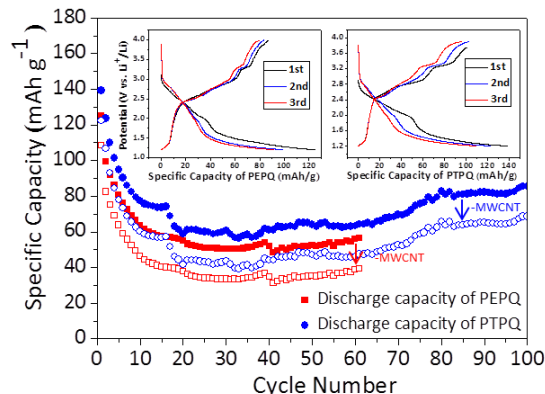

Figure 3. Cycling performance of PEPQ and PTPQ at 10 mA g^{-1}. Inset: discharge-charge curves of PEPQ and PTPQ at 10 mA g^{-1}.

As shown in Figure 3, PEPQ and PTPQ attained reasonable discharge capacities of 125 and 138 mAh g^{-1}, respectively, during the first discharge process at a current density of 10 mA g^{-1}. The capacity decayed over the first 20 cycles is possibly due to the dissolution of trace oligomers and/or the expansion effect of the cathode materials [28]. After 60 cycles, the reversible capacities of PEPQ and PTPQ were 56 mAh g^{-1} and 62 mAh g^{-1}. The capacities of both polymers increase gradually after 40 cycles, indicating the activation processes presented. The activation process is normal for both organic and inorganic cathode materials [29]. The capacity of PTPQ has a capacity of 86 mAh g^{-1} after 100 cycles. It has been previously reported that the insertion/de-insertion of lithium to/from carbon materials usually occurs in low potential regions at lower than 1.0 V relative to Li/Li^+ [30], and the controlled variable experiment indicated the contribution of MWCNT was about 17 mAh g^{-1}.
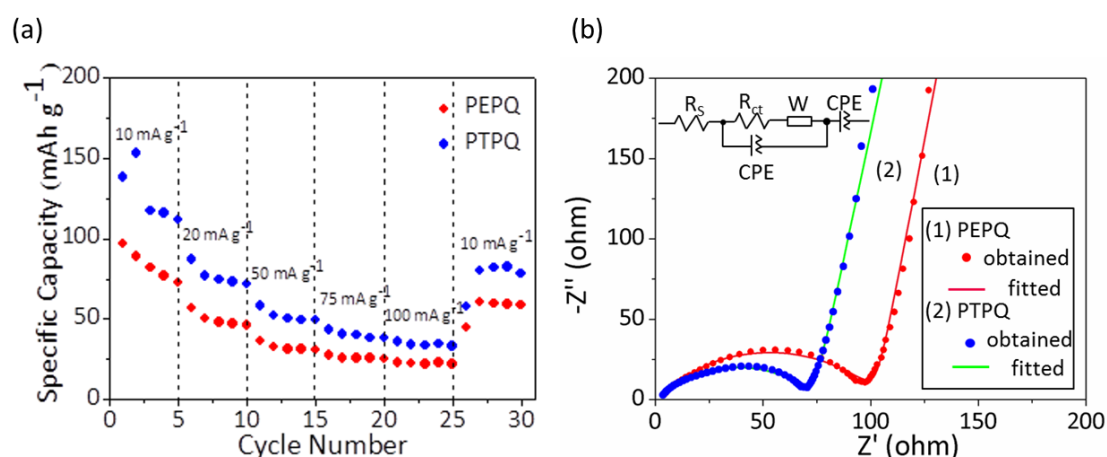

Figure 4. (a) Rate performance of PEPQ and PTPQ at 10, 20, 50, 75, and 100 mA g^{-1}. (b) EIS measurements of PEPQ and PTPQ. Inset: The equivalent circuit of PEPQ and PTPQ.

Rate performance tests were performed at progressively increasing current densities (10, 20, 50, 75, and 100 mA g^{-1}), as shown in Figure 4a. For the two cathode materials, the discharge capacities decreased with increasing current density, as expected. When the current density of the battery was reset to 10 mA g^{-1}, PEPQ could still maintain a capacity of 60 mAh g^{-1} (62% of the initial capacity). PTPQ achieved a better rate performance due to the introduction of thiophene units, which improved the material electronic conductivity [13]. Figure 4b shows the electrochemical impedance spectroscopy (EIS) analysis result of fresh PEPQ and PTPQ cells, with the frequency ranging from 10 kHz to 10 MHz (for a detailed analysis, see Table S1). Nyquist plots of the two cathode materials are presented by semicircles in the high- frequency regions which represent the charge transfer resistance (R_{ct}) and by straight lines in the low- frequency regions. Clearly, the R_{ct} value of PTPQ (73 Ω) is lower than that of PEPQ (101 Ω), implying that PTPQ has faster reaction kinetics. This result is correlated with the better behaviour of PTPQ mentioned earlier.

Table 1 describes the major performance parameters for the reported materials with the same functional moieties, in which the theoretical capacity, initial discharge specific capacity, capacity retention rate and material types are listed. By comparison, we can find that the cycling stabilities of

PEPQ and PTPQ were greatly improved through the polymerization strategy. The cyclability of the thiophene-alternated PTPQ is comparable to that of PhQ/SWCNTs, in which the functional PQ moieties were covalently grafted onto SWCNTs.

Table 1. Comparison of similar LIBs cathode materials

Sample	Theoretical capacity (mAh g^{-1})	Initial discharge capacity (mAh g^{-1}), current (mA g^{-1})	Cycles, retention	Material types	Ref.
PhQ-CB	258	148, 100	50th, 10%	PQ small molecule	[11]
PhQ-SWCNTs	258	171, 100	-	PQ small molecule	[11]
PhQ@SWCNTs	258	close to 258, 100	50th, 49%	PQ encapsulated in SWCNTs	[11]
PQ/CMK-3	258	220, 25.8	50th, 89%	PQ encapsulated in carbon materials	[18]
PhQ/SWCNTs	258	150, 100	100th, 70%	PQ covalently grafted onto SWCNTs	[30]
PFQ	260	158, 50	200th, 99%	Linear PQ polymer;	[14]
PFQ/rGO	260	200, 50	200th, 99%	Composite of PQ polymer/rGO	[14]
PEPQ PTPQ	231 185	125, 10 138, 10	60th, 45% 100th, 62%	Linear PQ polymer	This work

Based on the results above, the capacity of PTPQ attains an increase of 30 mAh g^{-1} over that of PEPQ, and the utilization rate of the active sites increase from 54% to 75%. We attribute the superior performance of PTPQ over PEPQ mainly to the higher electronic conductivity and faster (de)lithiation kinetics of the former. However, the highest capacity (138 mAh g^{-1}) of PTPQ still greatly differs from its theoretical value (185 mAh g^{-1}). The cycling stabilities of PTPQ and PEPQ are also unsuitable for practical applications. The possible swelling of the chain polymers during the charge/discharge processes might partially account for the insufficient cycling stabilities, which might be improved through the construction of cross-linked polymers with rigid backbones [14].

4. CONCLUSIONS

In conclusion, two novel organic polymers (PEPQ and PTPQ) embedded with densely and evenly distributed orthoquinone groups, known to have higher voltage potentials and faster electrochemical kinetics, were successfully synthesized from PQ, a coal tar component, which is available in large quantities. Beyond traditional anode materials from coal tar, PEPQ and PTPQ were studied as LIB cathode materials in this study, and a reversible specific capacity up to 138 mAh g^{-1} was achieved. The properties, such as experimental specific capacities and redox kinetics, of the PQ-based polymers can be tuned by structural design and post-modification with the incorporation of

chalcogen elements. This work supports that, by judicious structural design and facile synthetic methods, the properties of organic cathode materials can be rationally optimized through a bottom-up strategy. We note that the electrochemical performances of these type of materials are far from practical applications, especially the poor rate capabilities. However, the discovery in this work still offers elementary insights into the rational construction of organic electrode materials and the development of sustainable and eco-friendly electric energy storage devices.

SUPPLEMENTARY MATERIAL

This section includes:

1. EXPERIMENTAL SECTION

1.1 Materials and reagents
1.2 Synthesis

2. SUPPORTING FIGURES

3. THE CAPACITY CONTRIBUTION OF MWCNT

4. EIS DATA OF PEPQ AND PTPQ

1. EXPERIMENTAL SECTION

1.1 Materials and reagents

Phenanthrenequinone (99%), *N,N,N,N*-Tetramethylethylenediamine (TMEDA, 99%), *N*-Bromosuccinimide (NBS, >99%), *tert*-Butyldimethylchlorosilane (TBSCl, 98%), Copper(I) Iodide (99%), Ethynyltrimethylsilane (TMSA, >98%), Triethylamine (99%), Dichloromethane (98%), Potassium Fluoride (≥99%), Sodium *tert*-Butoxide (99%), Ceric Ammonium Nitrate (CAN, ≥98%) were purchased from Adamas; *N,N*-Dimethylformamide (DMF, ≥99.5%), Methyl Alcohol (≥99.5%), Hydrobromic Acid (48% solution in water), *tert*-Butanol (≥99%), *N*-Methyl-2-Pyrrolidinone (NMP, ≥99%), Potassium Carbonate (≥99%) were purchased from Greagent; Dichlorobis(Triphenylphosphine)Palladium(II) (98%) were purchased from TCI. Sulphur, concentrated Sulfuric Acid (H$_2$SO$_4$, >95%), zinc powder were purchased from Acros. Carbon nanotube bundled multi-walled (>90%, ID: 5-15 nm, OD: >50 nm, Length: 10-20 μm) were purchased from Macklin.
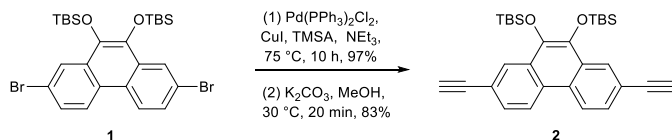
1.2 Synthesis

((2,7-dibromophenanthrene-9,10-diyl)bis(oxy))bis(tert-butyldimethylsilane) (1):

9,10-Phenanthraquinone (10.0 g, 48.0 mmol) and NBS (17.1 g, 96.0 mmol) were added in sequence to a 500-mL round bottom flask, then added 200 mL of concentrated sulfuric acid and stirred well. After reacting for 2 h at 25 °C, the product was slowly poured into an ice-water mixture. Then, the mixture was filtered out and dried in a vacuum oven, recrystallized in DMSO to give the product as orange solid (11.7 g, 32.0 mmol, 67%). ^{1}H NMR (500 MHz, DMSO-d_6) δ 8.26 (d, J = 8.6 Hz, 2H), 8.09 (d, J = 2.3 Hz, 2H), 7.97 (dd, J = 8.5, 2.3 Hz, 2H). Next, the obtained product (7.0 g, 19.1 mmol) and DMF (75 mL) were transferred into a 250-mL Schlenk tube under N_2. Then, Zn powder (18.9 g, 288.4 mmol), TBSCl (11.8 g, 78.3 mmol), TMEDA (14.1 mL, 93.6 mmol) were added in this order. After stirring at 35 °C for 11 h the reaction was completed, zinc powder residue was filtered out. White flocks were obtained after adding water to the flask, then filtered and washed with cold methanol. The obtained product was recrystallized in methanol to yield the product as white crystals (8.7 g, 14.6 mmol, 76%). ^{1}H NMR (400 MHz, CDCl$_3$) δ 8.36-8.39 (m, 4H), 8.62 (dd, J = 11.2 Hz, 2H), 1.15 (s, 18H), 0.09 (s, 12H). ^{13}C NMR (CDCl$_3$, 101 MHz): δ 137.59, 131.86, 128.40, 125.97, 125.89, 124.23, 120.95, 26.61, 18.91, -3.34; ESI-MS m/z calcd for $C_{26}H_{37}O_2Br_2Si_{27}$: 596.0699 [M+H]$^+$; found: 595.0707.
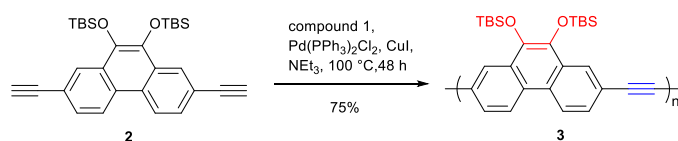
((2,7-diethynylphenanthrene-9,10-diyl)bis(oxy))bis(tert-butyldimethylsilane) (2):

To the 50-mL Schlenk tube was sequentially added compound 1 (4.0 g, 6.7 mmol), Pd(PPh$_3$)$_2$Cl$_2$ (140.4 mg, 0.2 mmol), CuI (38.1 mg, 0.2 mmol) under nitrogen protection, then added 22 mL of triethylamine and TMSA (2.2 mL, 15.4 mmol) dropwise successively. The reaction was heated to 75 °C and completed after 10 h. After extraction with DCM and brine, organic phases were combined and concentrated. The residue was purified by a short silica gel chromatography, and recrystallized in a mixture of dichloromethane and methanol (3.88 g, 6.5 mmol, 97%). ^{1}H NMR (400 MHz, CDCl$_3$) δ 8.44 (d, J = 8.5 Hz, 2H), 8.35 (d, J = 1.7 Hz, 2H), 7.57 (dd, J = 8.5, 1.7 Hz, 2H), 1.15 (s, 18H), 0.28 (s, 18H), 0.08 (s, 12H). ^{13}C NMR (CDCl$_3$, 101 MHz): δ 137.56, 130.48, 127.75, 127.05, 122.80, 121.15, 105.69, 94.99, 26.58, 18.97, 0.14, -3.35. ESI-MS m/z calcd for $C_{36}H_{55}O_2Si_4$: 631.3279 [M+H]$^+$; found: 631.3258. Next, the above product (2.0 g, 3.3 mmol) dissolved in 5 mL of DCM and added to a 500-mL round bottom flask, then the flask charged with K$_2$CO$_3$ (2.7 g, 19.8 mmol) and 33 mL of methanol sequentially. After 20 min, the color of the reaction system turned from orange to white. Extracted the organic phase with DCM and further separated and purified by silica gel chromatography. A light yellow powder was yielded (1.4 g, 2.8 mmol, 83%). ^{1}H NMR (400 MHz, CDCl$_3$) δ 8.48 (d, J = 8.5 Hz, 2H), 8.36 (d, J = 1.7 Hz, 2H), 7.62 (dd, J = 8.5, 1.7 Hz, 2H), 3.17 (s, 2H), 1.15 (s, 18H), 0.09 (s, 12H). ^{13}C NMR (CDCl$_3$, 101 MHz): δ 137.66, 130.54, 128.19, 127.58,
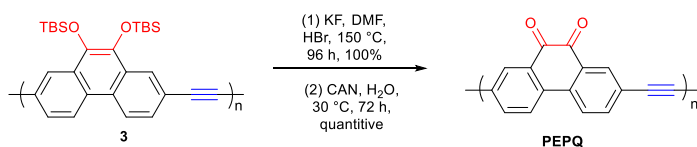
127.21, 122.94, 120.22, 84.07, 26.60, 18.91, -3.33. ESI-MS *m/z* calcd for $C_{30}H_{39}O_2Si_2$: 487.2489 [M+H]$^+$; found: 487.2439.
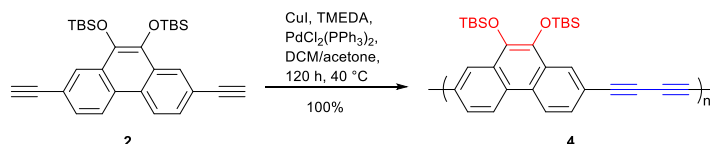
Compound 3:

The 100-mL Schlenk bottle was sequentially added compound 1 (0.5 g, 0.8 mmol), compound 2 (407.9 mg, 0.8 mmol), Pd(PPh$_3$)$_2$Cl$_2$ (28.1 mg, 0.04 mmol), and CuI (8.0 mg, 0.04 mmol) under nitrogen protection, then 6 mL of triethylamine was added. After reacting at 100 °C for 48 h, the precipitate in the flask was filtered out. The brown solid was washed successively with DCM, MeOH, H$_2$O, and dried in vacuum at 60 °C for 12 h to yield the product as a yellow solid (581.8 mg, 1.3 mmol, 75%). FTIR: 2920 cm^{-1}, 2860 cm^{-1}, 1580 cm^{-1}, 841 cm^{-1}. Elemental Analysis for $C_{28}H_{38}O_2Si_2$: Calculated: C, 72.67%; H, 8.28%. Found: C, 67.90%; H, 7.37%.

PEPQ:

Under nitrogen protection, KF (93.0 mg, 1.6 mmol), 5 mL of dried DMF, 48% HBr in water (0.01 mL, 0.04 mmol) were sequentially added to a 50-mL Schlenk tube, then placed the reaction bottle in an ice water bath. Compound 3 (0.1 g, 0.2 mmol) was added to the KF/HBr solution. After reacting at 150 °C for 96 h, 2 M cooled HCl was added dropwise to quench the reaction. The solid in the reaction flask was filtered out, washed successively with DCM, MeOH, H$_2$O, and dried in vacuum at 60 °C. A reddish brown solid was yielded (50.1 mg, 0.2 mmol, 100%). The obtained product was further oxidized by CAN. The product (0.1 g, 0.4 mmol) was added to a reaction bottle, and then added CAN (548.2 mg, 1.0 mmol) which dissolved in water. After stirring at 30 °C for 72 h, the obtained solid was washed with diluted HCl, H$_2$O, MeOH, and dried in vacuo at 60 °C overnight to yield the product as a red-brown solid (115 mg, 0.5 mmol). FTIR: 1678 cm^{-1}, 1602 cm^{-1}, 842 cm^{-1}. Elemental Analysis for $C_{16}H_8O_2$: Calculated: C, 82.75%; H, 3.47%. Found: C, 51.74%; H, 2.22%.
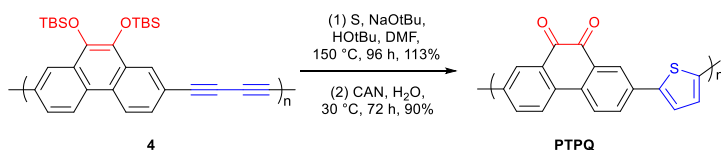
Compound 4:

Compound 2 (1.0 g, 2.1 mmol) dissolved in 40 mL of DCM/acetone mixed solvent ($V_{DCM}/V_{acetone}$ = 1:1, 40 mL), and added to a 250-mL reaction bottle, CuI (799.9 mg, 4.2 mmol) and 2.5 mL of TMEDA dissolved in DCM (10 mL) was added to the flask, then Pd(PPh$_3$)$_2$Cl$_2$ (140.4 mg, 0.2 mmol) was added. The system was refluxed under air for 120 h. The precipitate in the flask was filtered out, washed sequentially with DCM, MeOH, H$_2$O, and dried in vacuum at 60 °C for 12 h. A

yellow solid was yielded (1.0 g, 1.0 mmol, 100%). FTIR: 2920 cm^{-1}, 2850 cm^{-1}, 1590 cm^{-1}, 830 cm^{-1}. Elemental Analysis for $C_{30}H_{38}O_2Si_2$: Calculated: C, 74.02%; H, 7.87%. Found: C, 67.09%; H, 6.50%.

   PTPQ:

   In a Schlenk tube, compound 4 (0.1 g, 0.1 mmol), sulphur powder (9.6 mg, 0.3 mmol), and *t*-BuONa (57.7 mg, 0.6 mmol) in DMF/*t*-BuOH ($V_{DMF}/V_{t\text{-BuOH}}$ = 3:1, 2 mL) was stirred under N_2 at 150 °C. After 96 h the mixture was quenched with dilute HCl and filtered, the solid was washed three times with DCM, MeOH, H_2O, and dried in vacuo at 60 °C for 12 h. A black solid was yielded (70.0 mg, 0.2 mmol, 113%). The obtained product was further oxidized by CAN. The above product (0.1 g, 0.3 mmol) was added to a reaction bottle, then added CAN (438.6 mg, 0.8 mmol) which dissolved in water. After reacting at 30 °C for 72 h, the obtained solid was washed successively with dilute HCl, H_2O, MeOH, finally dried in a vacuum oven at 60 °C for 12 h to obtain a black powder solid (90.0 mg, 0.3 mmol, 90%). FTIR: 1673 cm^{-1}, 1600 cm^{-1}, 1043 cm^{-1}, 840 cm^{-1}. Elemental Analysis for $C_{18}H_{12}O_2S$: Calculated: C, 74.46%; H, 3.47%. Found: C, 58.52%; H, 3.02%.

2. SUPPORTING FIGURES
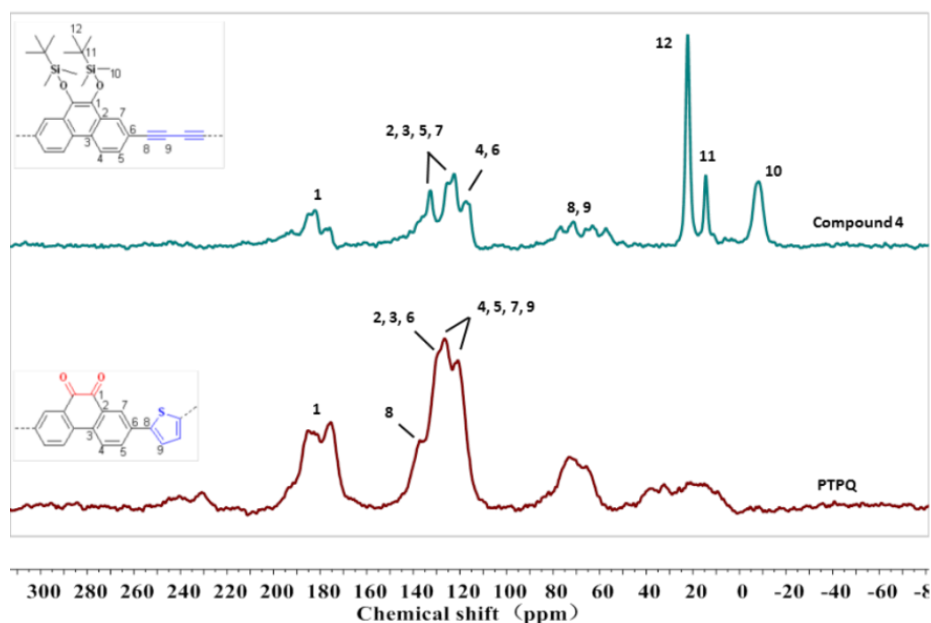

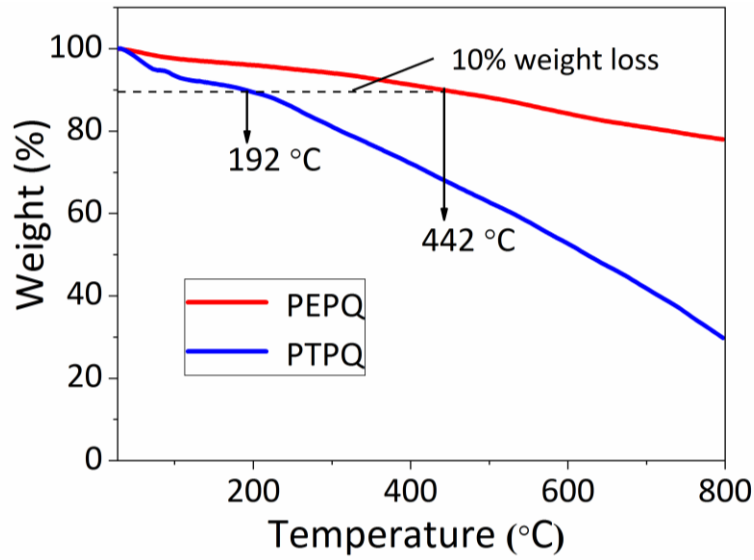**Figure S1.** Solid state ^{13}C CP/MAS NMR spectra of compound 4 and PTPQ.
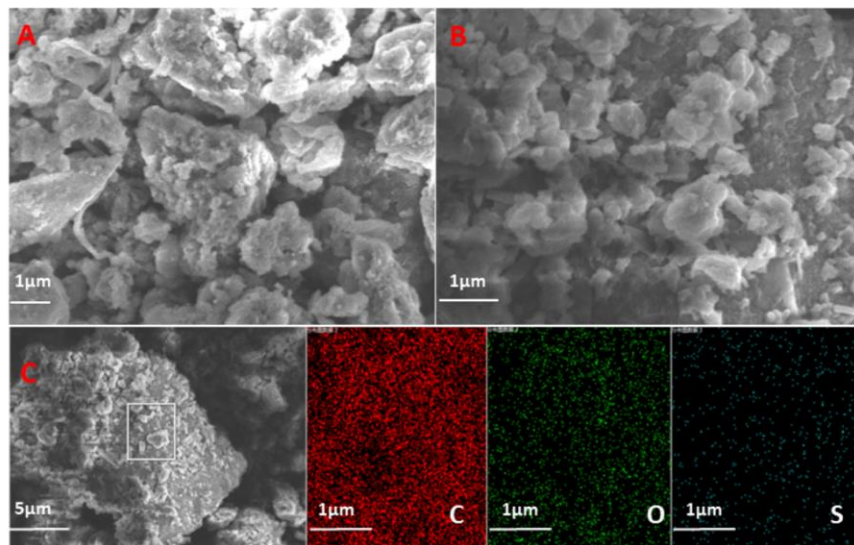
Figure S2. TGA analysis of PEPQ and PTPQ

Figure S3. SEM images of (A) PEPQ and (B) PTPQ (C) element mapping images of PTPQ

3. THE CAPACITY CONTRIBUTION OF MWCNT [14]

The real capacities of PEPQ and PTPQ are given by

$$C_{PEPQ} = C_{meas} - \frac{W_{CNT}}{W_{PEPQ}} C_{CNT} \qquad \text{(Equation S1)}$$

and

$$C_{PTPQ} = C'_{meas} - \frac{W_{CNT}}{W_{PTPQ}} C_{CNT} \qquad \text{(Equation S2)}$$

Where:

C_{PEPQ}, C_{PTPQ} — real capacities of PEPQ and PTPQ (mAh g^{-1})

C_{meas}, C'_{meas} — measured capacities of PEPQ and PTPQ (125 mAh g^{-1} and 138 mAh g^{-1}, respectively);

W_{CNT} — wt.% of multi-walled carbon nanotubes in electrode (50%);

W_{PEPQ}, W_{PTPQ} — wt.% of PEPQ or PTPQ in electrode (30%);

C_{CNT} — capacity of multi-walled carbon nanotubes (10 mAh g^{-1}).

4. EIS DATA OF PEPQ AND PTPQ

Table S1. R$_S$ and R$_{ct}$ of EIS data of PEPQ and PTPQ

	R$_S$/Ohm	R$_{ct}$/Ohm
PEPQ	2.38 Ω	101 Ω
PTPQ	1.22 Ω	73 Ω

In the equivalent circuit, R$_S$、R$_{ct}$、W and CPE represent solution resistance, charge transfer resistance, constant phase element, and Warburg impedance, respectively.

References

1. M. Armand, J. M. Tarascon, *Nature*, 451 (2008) 652.
2. X. Han, G. Qing, J. Sun, T. Sun, *Angew. Chem. Int. Ed.*, 51 (2012) 5147.
3. H. J. Kim, Y. Kim, J. Shim, K. H. Jung, M.S. Jung, H. Kim, J. C. Lee, K. T. Lee, *ACS Appl. Mater. Interfaces,* 10 (2018) 3479.
4. H. Chen, M. Armand, G. Demailly, F. Dolhem, P. Poizot, J. M. Tarascon, *ChemSusChem*, 1 (2008) 348.
5. Q. Zhao, Z. Zhu, J. Chen, *Adv. Mater.*, 29 (2017) 1607007.
6. Y. Liang, P. Zhang, J. Chen, *Chem. Sci.*, 4 (2013) 1330.
7. D. Larcher, J. M. Tarascon, *Nat. Chem.*, 7 (2014) 19.
8. Y. Zhang, J. Wang, S. N. Riduan, *J. Mater. Chem. A*, 4 (2016) 14902.
9. A. L. Comte, D. Chhin, A. Gagnon, R. Retoux, T. Brousse, D. Bélanger, *J. Mater. Chem. A*, 3 (2015) 6146.
10. K. Pirnat, R. Dominko, R. Cerc-Korosec, G. Mali, B. Genorio, M. Gaberscek, *J. Power Sources*, 199 (2012) 308.
11. Y. Ishii, K. Tashiro, K. Hosoe, A. Al-zubaidi, S. Kawasaki, *Phys. Chem. Chem. Phys.*, 18 (2016)

10411.

12. F. Xu, J. Xia, W. Shi, *Electrochem. Commun.*, 60 (2015) 117.
13. J. Xie, W. Chen, G. Long, W. Gao, Z. J. Xu, M. Liu, Q. Zhang, *J. Mater. Chem. A*, 6 (2018) 12985.
14. K. Pirnat, J. Bitenc, A. Vizintin, A. Krajnc, E. Tchernychova, *Chem. Mater.*, 30 (2018) 5726.
15. T. Nokami, T. Matsuo, Y. Inatomi, N. Hojo, T. Tsukagoshi, H. Yoshizawa, A. Shimizu, H. Kuramoto, K. Komae, H. Tsuyama, J. Yoshida, *J. Am. Chem. Soc.*, 134 (2012) 19694.
16. J. Zhao, J. Yang, P. Sun, Y. Xu, *Electrochem. Commun.*, 86 (2017) 34.
17. A. E. Lakraychi, K. Fahsi, L. Aymard, P. Poizot, F. Dolhem, J. -P. Bonnet, *Electrochem. Commun.*, 76 (2017) 47.
18. M. S. Kwon, A. Choi, Y. Park, J. Y. Cheon, H. Kang, Y. N. Jo, Y. J. Kim, S. Y. Hong, S. H. Joo, C. Yang, *Sci. Rep.*, 4 (2014) 7404.
19. G. Zhang, Z. Xu, P. Liu, Y. Su, T. Huang, R. Liu, X. Xi, D. Wu, *Electrochim. Acta*, 260 (2018) 598.
20. D. J. Kim, D. -J. Yoo, M. T. Otley, A. Prokofjevs, C. Pezzato, M. Owczarek, S. J. Lee, J. W. Choi, J. F. Stoddart, *Nat. Energy*, 4(2018) 51.
21. D. J. Kim, K. R. Hermann, A. Prokofjevs, M. T. Otley, C. Pezzato, M. Owczarek, J. F. Stoddart, *J. Am. Chem. Soc.*, 139 (2017) 6635.
22. Z. Song, Y. Qian, M. L. Gordin, D. Tang, T. Xu, M. Otani, H. Zhan, H. Zhou, D. Wang, *Angew. Chem. Int. Ed.*, 54 (2015) 13947.
23. G. Li, B. Zhang, J. Wang, H. Zhao, W. Ma, L. Xu, W. Zhang, K. Zhou, Y. Du, G. He, *Angew. Chem. Int. Ed.*, 58 (2019) 8468.
24. C. Xu, Characteristics and processing utilization of coal tar, *Clean Coal Technol.*, 19 (2013) 63.
25. C. Zhang, Y. He, P. Mu, X. Wang, Q. He, Y. Chen, J. Zeng, F. Wang, Y. Xu, J. Jiang, *Adv. Funct. Mater.*, 28 (2018) 1705432.
26. R. Zeng, X. Li, Y. Qiu, W. Li, J. Yi, D. Lu, C. Tan, M. Xu, *Electrochem. Commun.*, 12 (2010) 1253.
27. K. Nakahara, S. Iwasa, M. Satoh, Y. Morioka, J. Iriyama, M. Suguro, E. Hasegawa, *Chem. Phys. Lett.*, 359 (2002) 351.
28. J. Bitenc, K. Pirnat, T. Bancic, M. Gaberscek, B. Genorio, A. Randon-Vitanova, R. Dominko, *ChemSusChem*, 8 (2015) 4128.
29. H. Kang, H. Liu, C. Li, L. Sun, C. Zhang, H. Gao, J. Yin, B. Yang, Y. You, K. Jiang, H. Long, S. Xin, *ACS Appl. Mater. Interfaces*, 10 (2018) 37023.
30. L. Canghao, N. Motoumi, I. Shunya, I. Yosuke, K. Shinji, A. Al-zubaidi, S. Kento, H. Yoshiyuki, *ACS Omega*, 3 (2018) 15598.